Meteorol. Atmos. Phys. 36, 215–227 (1987)

Meteorology and Atmospheric Physics

551.555.4

[1] National Center for Atmospheric Research, Boulder, Colorado, U.S.A., and
[2] University of Utah, Salt Lake City, Utah, U.S.A.

Numerical Modelling of Bora Winds

J. B. Klemp[1] and **D. R. Durran**[2]

With 12 Figures

Received January 27, 1985

Summary

The Bora winds are produced by cold stable air which pours over the Dinaric Alps, often producing intense winds along the Adriatic Coast. Although the flow appears qualitatively similar to the hydraulic flow described by the shallow-water equations, there are certain significant differences: the cold low-level air is continuously stratified and a critical layer in the winds typically occurs near the inversion which caps the cold pool of air. Through two-dimensional numerical mountain wave simulations, we investigate the extent to which hydraulic theory can be used to describe the Bora winds. We analyze the structure of the Bora flow derived from aircraft observations collected during the ALPEX field phase on 15 April 1982 and compare it with a numerical simulation initialized from upstream sounding data. By varying the environmental sounding in our simulations, we find that for this case, neither the critical layer nor the inversion layer play a fundamental dynamical role in generating the strong winds along the lee slope. Instead, the wave overturning which occurs beneath the inversion appears to be the most important factor in producing the strong response. This overturning produces shooting flow over the lee slope and strongly resembles the hydraulic flow which occurs both in shallow water theory and in simulations in which overturning is suppressed. We believe the hydraulic jump-like mechanism producing the strong Bora slope winds is fundamentally similar to the underlying mechanism which produces the intense winds along the lee slope of the Rocky Mountains. This occurs despite significant differences in the character of the larger scale flow in these two situations.

Zusammenfassung

Numerische Modellierung der Bora

Die Borawinde entstehen durch kalte, stabile Luft, die über die Dinarischen Alpen fließt und dabei oft heftige Winde entlang der adriatischen Küste erzeugt. Obwohl die Strömung der mit Hilfe der Seichtwassergleichungen beschriebenen hydraulischen Strömung qualitativ ähnlich ist, gibt es bestimmte, signifikante Unterschiede: die kalte, bodennahe Luft ist kontinuierlich geschichtet und charakteristischerweise befindet sich eine kritische Windschicht nahe der Inversion, die den Kältesee abschließt. Mittels zweidimensionaler, numerischer Gebirgswellensimulationen untersuchen wir, in welchem Ausmaß die hydraulische Theorie zur Beschreibung von Borawinden herangezogen werden kann. Wir analysieren die Struktur der Boraströmung, die während der ALPEX-Meßphase am 15. April 1982 vom Flugzeug aus beobachtet wurde, und vergleichen sie mit einer numerischen Situation, die mit Daten aus einer Sondierung im Anströmgebiet initialisiert wird. Durch Variieren der Sondierung in den Simulationen haben wir herausgefunden, daß in diesem Fall weder die kritische noch die Inversionsschicht eine fundamentale dynamische Rolle bei der Entstehung der heftigen Winde entlang des leeseitigen Hanges spielen. Stattdessen scheint die umschlagende Welle unterhalb der Inversion der wichtigste Faktor bei der Erzeugung dieser heftigen Reaktion zu sein. Dieses Umschlagen erzeugt eine sehr schnelle Strömung über dem leeseitigen Hang und gleicht damit stark der hydraulischen Strömung, die sowohl in der Seichtwassertheorie vorkommt, als auch in Simulationen, in denen das Umschlagen unterdrückt wird. Wir glauben, daß der dem "hydraulic jump" ähnliche Mechanismus,

der die heftigen Borahangwinde hervorruft, grundsätzlich dem Mechanismus gleicht, der die heftigen Winde entlang der leeseitigen Hänge der Rocky Mountains erzeugt. Und das, obwohl signifikante Unterschiede in den Eigenschaften der großräumigen Strömung in diesen beiden Situationen bestehen.

1. Introduction

Bora winds frequently occur along the Adriatic Coast in Yugoslavia when cold stable air advances through Eastern Europe and pours over the Dinaric Alps. The onset of the Bora wind is generally accompanied by a dramatic decrease in temperature and the lee slope winds may be intense and damaging. Brinkman (1973), in summarizing the climatology of mountain winds, noted that:

> At Trieste, for instance, gust speeds of over 30 m s^{-1} are quite frequent and occasionally exceed 50 to 60 m s^{-1}. The wind is known to have lifted roofs, swept people off their feet and stopped traffic because of the many accidents caused by overturned automobiles, street cars, and even trains; ropes are stretched along sidewalks for use by pedestrians.

Although the synoptic conditions associated with Bora events have been studied extensively (cf. Yoshino 1976), the detailed structure of the flow was not documented until instrumented aircraft flights were conducted over the Adriatic Coast during the Special Observing Period of the Alpine Experiment (ALPEX) during March–April 1982. In a preliminary analysis of these aircraft data (Smith 1982) the Bora displays strong similarities to hydraulic flows which become supercritical over the crest of the mountain, accelerate down the lee slope, and then dissipate their energy within a hydraulic jump. Such hydraulic jump models have been previously proposed to explain the strong downslope winds which occur in many parts of the world (Long 1953 and Kuettner 1959, for Sierra Nevada winds; Ball 1956, for Antarctic slope winds; Schweitzer 1953, for the Alpine föhn; Arakawa 1969, for winds on Hokkaido, Japan).

There are some striking similarities between the Bora and hydraulic flows described by the shallow-water equations. This may be due to the presence of a strong inversion layer above the cold low-level air, which could behave in a similar fashion to the discontinuity in density at a layer interface in hydraulic theory. However, there are also significant differences between the atmospheric conditions which are typically observed during Bora events and those generally assumed in hydraulic theory. In the Bora, the cold low-level air is continuously stratified, while the stability is assumed to be zero throughout each layer of fluid in hydraulic theory. In both cases, there is little vertical propagation of wave energy; however, in hydraulic theory, the reflective free surface boundary condition (or, in some cases, a rigid lid) prohibits vertical energy propagation, whereas in the Bora, this propagation is restricted by a critical layer (a level at which the cross-mountain wind reverses direction) which typically occurs near the top of the inversion capping the pool of cold air. In this study, we will use a two-dimensional numerical model to investigate the principal environmental factors that produce strong Bora winds, and evaluate the extent to which they are included in hydraulic theory.

We begin, in section 2, by presenting a brief analysis of the Bora flow as derived from the ALPEX aircraft and sounding data collected on 15 April 1982. In section 3, we describe the model simulation for this case, followed, in section 4, with simulation experiments in which either the critical layer or the inversion layer is selectively removed. Perhaps surprisingly, these results suggest that in this case, neither the critical layer nor the inversion layer play a fundamental role in generating the strong winds along the lee slope. Rather, wave overturning beneath the inversion appears to be primarily responsible for the strong shooting flow and jump-like recovery which develop along the lee slope. In section 5, we present further sensitivity experiments conducted with idealized soundings. These simulations illustrate that if wave overturning is suppressed, the response varies with the Froude number in a manner which is quite similar to that predicted by hydraulic theory. In the discussion in section 6, we speculate that the hydraulic jump-like mechanism producing

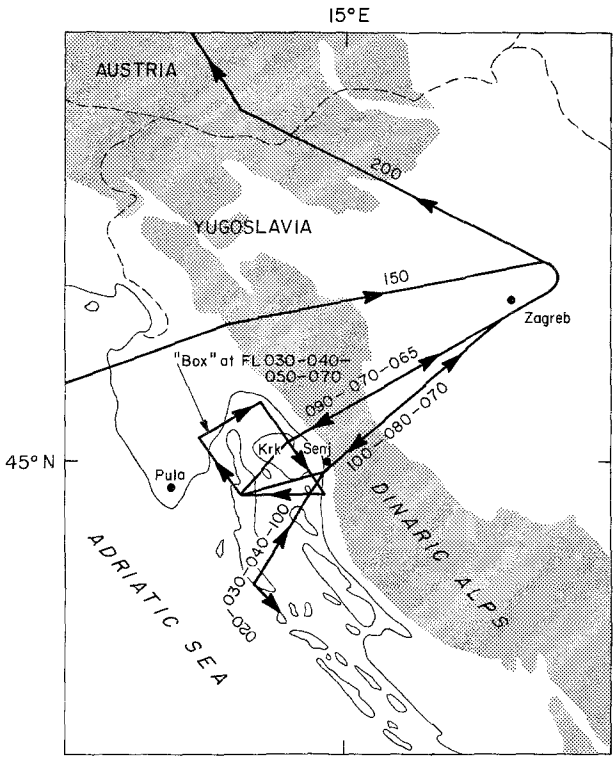

Fig. 1. Aircraft flight tracks for ALPEX flight P415 over the Dinaric Alps on 15 April 1982. Labels along flight legs indicate the altitude in hundreds of feet. Shaded areas indicate elevations above 2000 ft (from ALPEX Flight Atlas, Kennedy 1982)

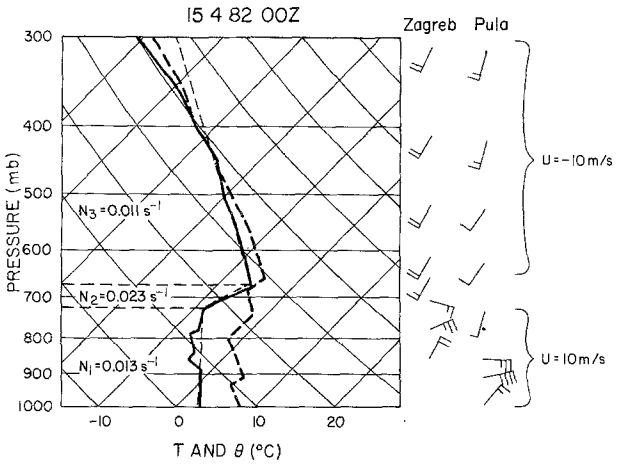

Fig. 2. Thermodynamic soundings at 00z 15 April 1982 from Zagreb (heavy solid line) and Pula, Yugoslavia (heavy dashed line). Wind barbs for both Zagreb and Pula are displayed in kts. The upstream sounding used in the numerical simulation is indicated by a light dashed line

the strong Bora winds may be fundamentally similar to the underlying mechanism which produces the intense winds along the lee slope of the Rocky Mountains. This may occur despite significant differences in the character of the larger scale flow in these two situations.

2. Observed Bora Flow on 15 April 1982

During the period 12–15 April 1982, moderate to strong Bora winds occurred along the Adriatic Coast. On the morning of 15 April, the NOAA P-3 flew a mission (ALPEX mission P415) to document the structure of the airflow over the Dinaric Alps and the Adriatic Coast southwest of Zagreb, Yugoslavia. Fig. 1 displays an overall summary of the flight tracks. Cross-mountain tracks were flown along two cross sections; the first section began at Zagreb and passed over the Island of Krk in the Adriatic (Zagreb-Krk section), while the second, aligned between Zagreb and Senj on the coast (Zagreb-Senj section) was displaced further to the south. In addition, a number of flight legs and box patterns were flown over the Adriatic Coast to document three-dimensional aspects of the flow. These data suggest that the cross-mountain flow had a stronger two-dimensional character along the Zagreb-Krk section (Smith 1982). In our brief discussion of the Bora structure for this case, we shall consider only the flow along the Zagreb-Krk section.

The atmospheric soundings on 00z April from Zagreb and Pula, Yugoslavia, shown in Fig. 2, document the environmental flow approximately 110 km upstream and downstream of the mountain ridge (based on the low level flow), respectively. The Zagreb sounding reveals the pool of cold, relatively stable air capped by a strong inversion at about 700 mb. Beneath the inversion, the winds are from the northeast at about 10 m s^{-1} while above the inversion the wind direction is reversed. Consequently, a critical layer for stationary disturbances accompanies the inversion in the mesoscale environment. The Pula sounding suggests there has been a net lowering of the lower portion of the inversion layer as well as of the air beneath it. The Pula wind profile also exhibits a critical layer as well as accelerated low-level winds.

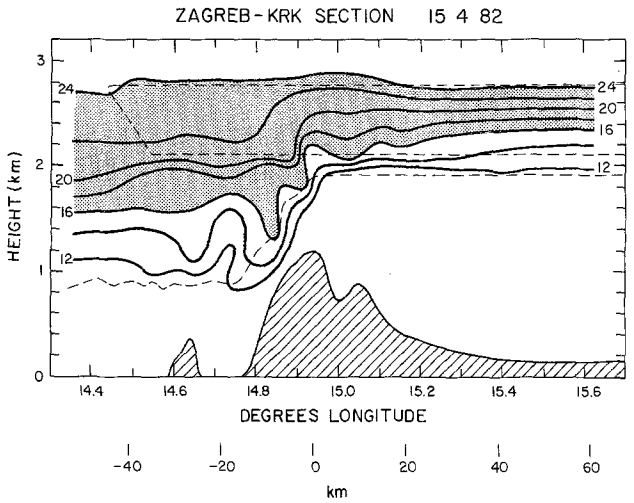

Fig. 3. Potential temperature contours over the Dinaric Alps on 15 April 1982, as derived from aircraft data. The vertical cross section extends to the southeast at an approximate 235° heading, passing over the Island of Krk just off the Adriatic Coast (Zagreb-Krk section). Contours are interpolated from data recorded along three traverses (thin dashed lines) and also using information from flight legs over the Adriatic, parallel to the Coast at altitudes of 1180, 1480 and 2140 m, where they intersected this vertical cross section. The location of the inversion layer as it passes over the mountain is indicated with light shading

The vertical cross section of potential temperature, shown in Fig. 3, is derived from the three cross-mountain flight tracks along the Zagreb-Krk section plus data from flight legs over the Adriatic which intersected this plane. To the extent that the flow is nearly steady, inviscid, and two-dimensional, these potential temperature contours also represent streamlines of the flow. This cross section reveals the strong descent of the cold, lower-level air over the lee slope of the mountain ridge. However, notice that while the lower portion of the inversion layer is part of the descending air stream. the upper portion remains relatively undisturbed. Higher level data from the Zagreb-Senj section, and also from other Bora flights during ALPEX, suggest that there is little wave activity above the inversion.

3. Numerical Simulation of the Bora Flow

We have simulated the 15 April 1982 Bora numerically using the two-dimensional, non-hydrostatic model of the fully compressible equations described by Durran and Klemp (1982, 1983). The model has a transformed vertical coordinate to accommodate the variable height terrain, open lateral boundaries, and a radiation condition at the upper boundary (Klemp and Durran 1983) to minimize artificial gravity wave reflections. For these simulations, we have specified a domain which encompasses 200 km in the horizontal with a 2 km grid size, and 8 km in the vertical with a 200 m grid interval. To approximate the terrain shape (see Fig. 3), we use a bell-shaped mountain profile which has a 1200 m maximum height, a half-width of 20 km on the upwind side and 10 km on the lee side. In this model, the low-level flow is from left to right, so the cross sections shown will be reversed from the observed section displayed in Fig. 3.

We initialize the numerical model using temperature and wind data based on the 00z 15 April Zagreb sounding. For the potential temperature, we specify a three-layer structure, shown by the thin dashed line in Fig. 2, having a Brunt-Väisälä frequency $N_1 = .0139\ s^{-1}$ below the inversion, $N_2 = .0239\ s^{-1}$ within the 600 m deep inversion layer, and $N_3 = .0110\ s^{-1}$ above. Since the mountain ridge is oriented nearly northwest to southeast, the horizontal winds shown in Fig. 2 are aligned approximately perpendicular to the ridge (northeast-southwest), both below and above the inversion. Thus, we initialize the horizontal wind U such that $U = 10\ m\ s^{-1}$ below the inversion, U varies linearly from 10 m s^{-1} to $-10\ m\ s^{-1}$ over a 1 km deep layer beginning at the base of the inversion, and $U = -10\ m\ s^{-1}$ above. With this profile, the initial wind reverses sign just below the top of the inversion.

Contours of the potential temperature and horizontal wind fields after 20 000 s (about 5.5 h) of numerical integration are shown in Fig. 4. The simulated isentropes display a structure which is similar to the observed flow in Fig. 2. Notice, however, that during the 5–6 h interval between the 00z sounding and the aircraft flights along this section, the inversion layer has lowered by about 300 m. We have also simulated this case with a sounding in which the inversion is lower by 300 m, and the result

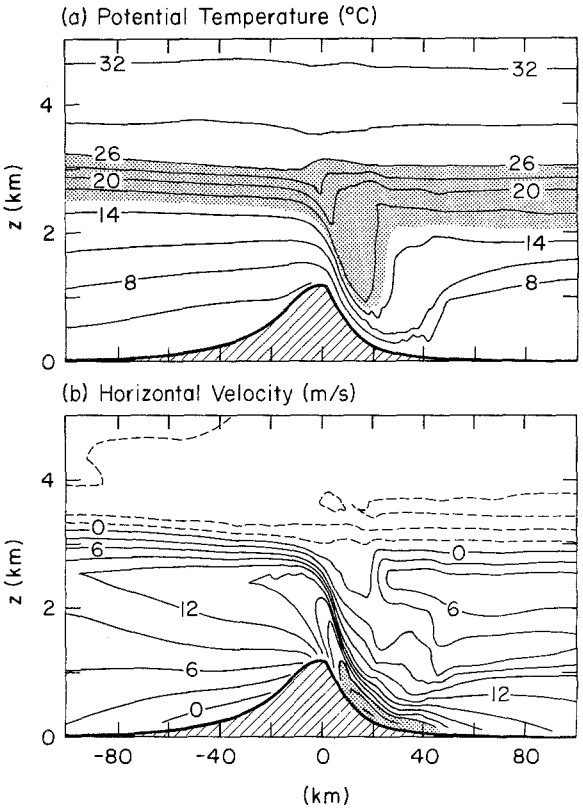

Fig. 4. Structure of Bora flow from a numerical simulation based on the 00z 15 April 1982 Zagreb sounding. (a) Potential temperature contours in °C with inversion layer shaded and (b) horizontal velocity contours in m s^{-1} with shading to highlight the region in which $u > 24$ m s^{-1}

is very similar to that shown in Fig. 4, except that the inversion and critical layers are proportionately lower.

As in the observed flow, the lower portion of the inversion descends over the lee slope while the upper portion passes over the mountain ridge relatively undisturbed. In the sharply descending airstream, the contours of horizontal velocity are nearly parallel to the isentropes, and at the surface these winds reach a maximum of 30 m s^{-1}. The lee-slope winds recorded along the flight track (not shown) were not particularly strong. This is not surprising since the simulated winds exceed 15 m s^{-1} only within about 500 m of the surface, while the lowest flight track on the lee side was at about 870 m (see Fig. 3). However, flight observers commented on the evidence of strong winds at the sea surface, made visible by large white caps moving away from the shore.

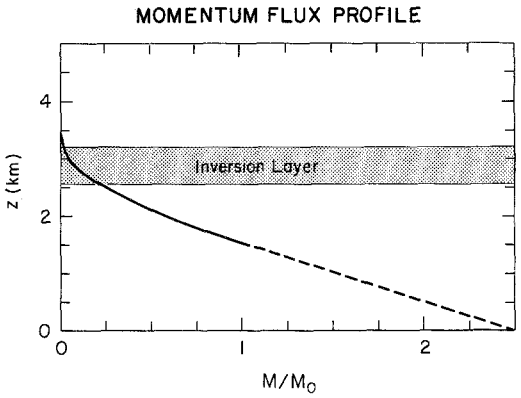

Fig. 5. Vertical flux of horizontal momentum for the simulated Bora flow. The portion of the profile interpolated to match the pressure drag at the surface is indicated by the dashed portion of the line

The profile for the vertical flux of horizontal momentum is shown in Fig. 5. This flux is normalized by the momentum flux

$$M_0 = \frac{\pi}{4} \rho_0 N_1 U_1 H_m^2$$

for the linear hydrostatic flow of a uniform atmosphere with the same properties as those below the inversion layer (N_1 =.0139 s^{-1}, U_1 = 10 m s^{-1}) over a bell shaped mountain of height H_m = 1200 m. Here, ρ_0 is a reference density at the surface. We computed the momentum flux at levels above the top of the mountain, and interpolated the profile to the surface value given by the surface pressure drag drag. Strong momentum flux divergence occurs throughout the layer beneath the inversion and the vertical transport is virtually zero at the top of the inversion.

4. Influence of the Inversion and Critical Layers on the Simulated Bora Structure

What are the important environmental factors that produce these strong Bora events? As mentioned in the previous section, the Zagreb sounding exhibits two significant features: a strong inversion layer and a critical layer. To evaluate the influences of these features on the flow structure, we recomputed the numerical simulations with altered initial soundings, in which (a) the critical layer is removed by speci-

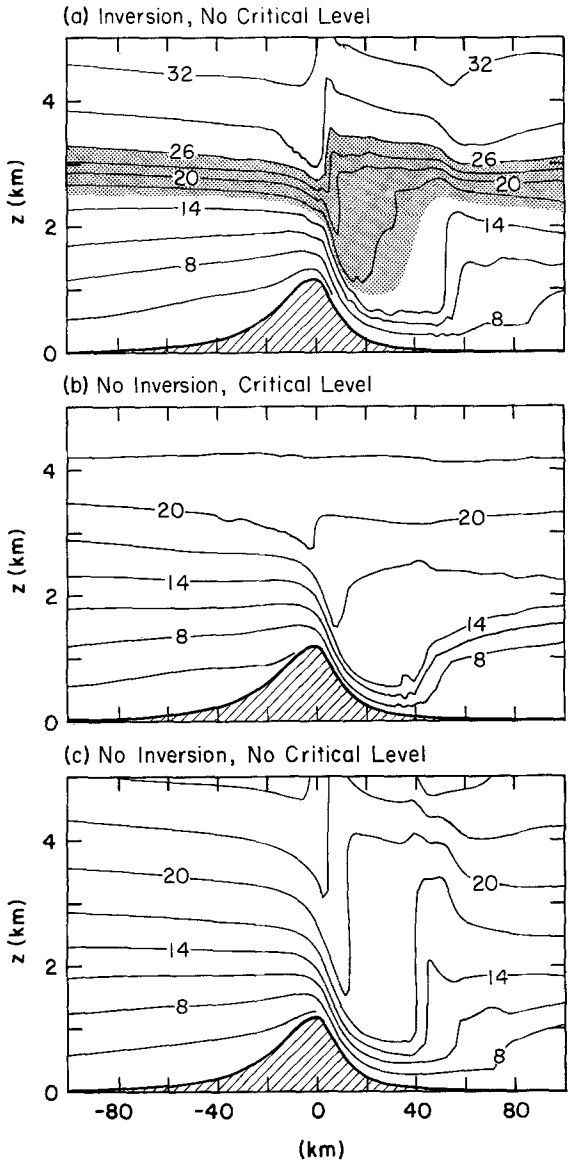

Fig. 6. Potential temperature contours (in °C) for numerical simulations as shown in Fig. 4a, except that the initial sounding has been altered so that: (a) the critical layer has been removed, (b) the inversion layer has been removed, and (c) both the critical layer and the inversion layer have been removed. The shaded region in (a) depicts the location of the stable layer

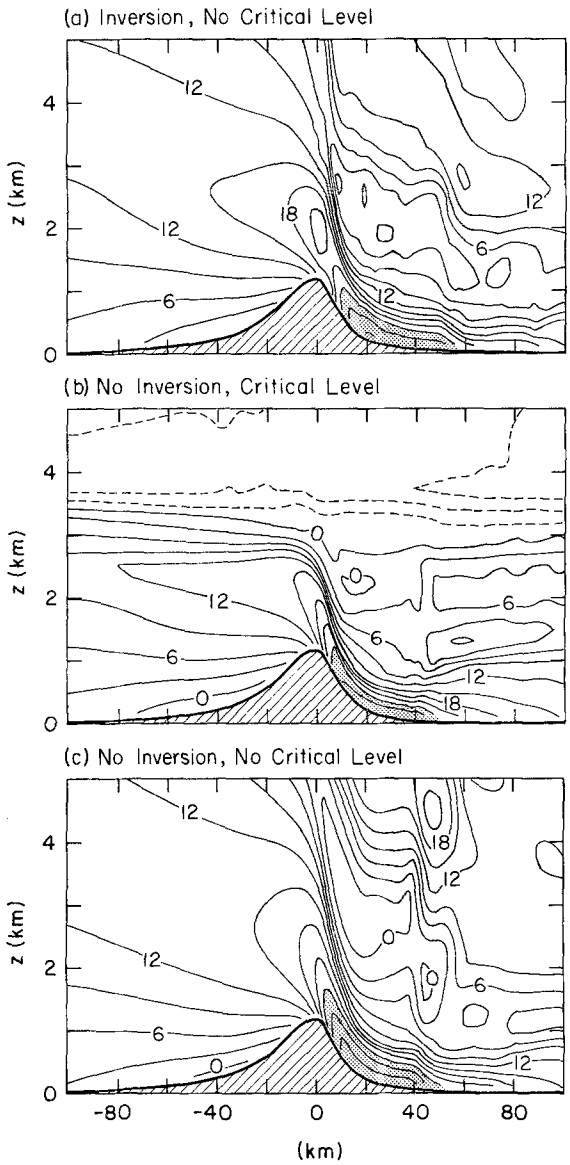

Fig. 7. As in Fig. 6, except for horizontal velocity (in m s^{-1}). The regions in which $u > 24$ m s^{-1} are shaded

fying $U = 10$ m s^{-1} everywhere, (b) the inversion layer is removed by setting $N_2 = N_3 = .0110\,s^{-1}$, and (c) the inversion layer and critical layer are both removed. The potential temperature and horizontal wind fields for these simulations are displayed in Figs. 6 and 7, respectively.

Consider first the simulation with a constant initial wind field shown in Figs. 6a and 7a. Comparing this flow structure to the reference simulation in Fig. 4, we see that without the critical layer, the inversion is more highly perturbed and a standing wave persists above the inversion layer. Thus, in this case, the critical layer is acting primarily as a wave absorbing region which effectively removes the upward propagating wave energy. However, notice that the low level flow structure, and the horizontal wind field especially, is nearly unchanged. When the critical layer is retained while the inversion is removed (Figs. 6b and 7b), the low-level struc-

ture is again very similar to the reference simulation, and as before, there is little evidence of wave activity above the critical layer. Finally, when both the inversion and critical layers are removed (so that the wind speed is uniform and there is only a small difference in stability between the lower and upper layers), wave activity reappears at higher levels (Figs. 6c and 7c), but the structure of the shooting flow and strong winds along the lee slope remains similar to that in the other simulations.

The insensitivity of the low-level flow structure to these variations in the environmental sounding suggests that, at least in this case, neither the inversion layer nor the critical layer plays a fundamental dynamical role in producing the strong lee slope response. Rather, it appears that wave breakdown occurs at levels beneath these layers and that this breakdown is responsible for the greatly accelerated flow along the lee slope. Within the lowest layer the parameter $N_1 H_m / U_1$ is 1.67, which is more than double the amplitude required to produce wave overturning in an atmosphere having constant N_1 and U_1 flowing over a mountain with this asymmetric shape (see Lilly and Klemp 1979). This low-level wave breakdown is also consistent with the large momentum-flux divergence beneath the inversion/critical layer that is apparent in Fig. 5. Previous mountain wave modelling studies (cf. Peltier and Clark 1979; Durran and Klemp 1983) have also documented the development of a low-level shooting flow in the lee of the mountain following wave overturning aloft.

We have also conducted Bora simulations in which the inversion/critical layer in the reference sounding was raised or lowered. These results are consistent with those shown in Fig. 6; if the layer was raised, the wave amplitude beneath the inversion increased (becoming increasingly similar to the structure shown in Fig. 6c), while the low-level flow remained essentially unchanged. If the layer was lowered, the low-level flow structure was significantly altered when the inversion/critical layer was located beneath the overturning layer (this situation will be discussed further in the next section).

In spite of the results desribed above, we do not believe that the inversion layer is unimportant in promoting a strong Bora flow. If wave overturning does not occur beneath it, the inversion will be a crucial factor determining the response, as demonstrated in the next section. Even in this 15 April 1982 case, it is likely that the pool of cold air upstream of the Dinaric Alps is largely responsible for producing the cross-mountain flow beneath the inversion (see also Smith 1982). To illustrate this influence, we have also simulated this case beginning with an artificial initial state in which there is no wind and the initial temperature field is specified by the 00z Zagreb sounding to the left of the mountain crest, while to the right, it is calculated by continuing the upper level stability (N_3 =.011 s^{-1}) down to the ground. Thus, the cross-mountain flow is initially generated by horizontal pressure gradients arising from the horizontal inhomogeneity in temperature. The resulting flow structure, shown in Fig. 8, is very similar qualitativey to the forced flow initiation (see Fig. 4) and is, perhaps, in even better agree-

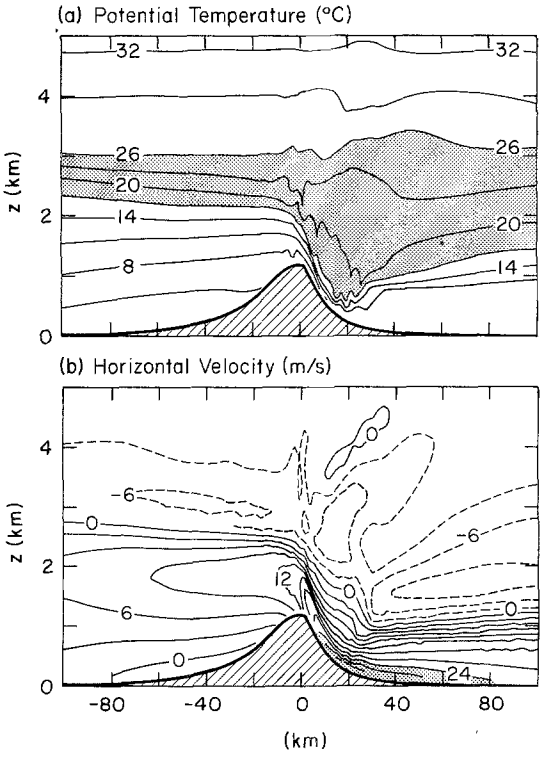

Fig. 8. As in Fig. 4, except for altered initial conditions in which there is no wind and the cold air pool exists only on the upstream side of the mountain, as described in the text

ment with the observed flow in Fig. 3. In Fig. 8, the lower portion of the inversion recovers only gradually (as observed) after descending over the lee slope, and there is a reversal in the wind direction at the 2 km level on the lee side of the mountain which is similar to that recorded along the 7000 ft (2140 m) flight leg.

5. Similarities of Bora Structure to Hydraulic Flow

When wave overturning does not occur beneath the inversion layer, the inversion may strongly modulate the low-level flow structure. This situation can arise when the wave amplitude within the lowest layer is insufficient to induce overturning, or when the inversion is located beneath the level at which overturning would occur. In these cases, our model simulations closely resemble the solutions calculated from hydraulic theory.

In order to evaluate the nature of the flow under these circumstances, we further simplified the atmospheric sounding used in the previous sections. We specified a constant mean with $U = 20$ m s^{-1}, thereby removing the critical layer and reducing NH_m/U in the lowest layer. In addition, we altered the three layer stability profile so that $N_1 = N_3 = .011$ s^{-1}, while retaining $N_2 = .0239$ s^{-1} in the inversion, but increasing its thickness to 1 km. For these atmospheric conditions, $N_1 H_m/U = .65$, which (ignoring compressiblity effects) would be below the overturning value for this mountain.

In Figs. 9 and 10, we display the potential temperature and horizontal wind fields at $t = 20\,000$ s for simulations with the inversion layer located at 4 different heights: (a) 1200–2200 m, (b) 2200–3200 m, (c) 3200–4200 m, and (d) 4200–5200 m. With the inversion base at mountain top level (Figs. 9a and 10a), the inversion layer descends abruptly over the lee slope and the surface winds remain high at large distances downstream of the mountain. When we raise the height of the inversion by 1 km (Figs. 9b and 10b), the inversion again descends sharply in the lee, but then recovers farther downstream in a jump-like fashion. Raising the inversion layer by another km (Figs. 9c and 10c) produces as jump-like recovery above the lee slope with the region of high surface winds localized in the immediate lee of the mountain. With the base of the inversion at 3 km above the mountain crest (Figs. 9d and 10d), the inversion layer is perturbed much less as it traverses the mountain and no intense winds occur along the lee slope.

These simulations reveal flow structures which bear strong visual similarities to hydraulic flows. To pursue this analogy further, we have computed corresponding solutions to the two-dimensional shallow water equations

$$\frac{\partial \phi}{\partial t} + \frac{\partial u\phi}{\partial x} + g'h\frac{\partial}{\partial x}(h + h_m) = K\frac{\partial^2 \phi}{\partial x^2}, \quad (1)$$

$$\frac{\partial h}{\partial t} + \frac{\partial \phi}{\partial x} = 0, \quad (2)$$

where u is the horizontal velocity within the shallow water layer, h is thickness of the layer, $\phi = uh$ is the momentum, and h_m is the height of the mountain contour.

As applied to the atmosphere, the shallow water equations describe hydrostatic flow within a neutrally stable layer in which variations in velocity across the layer can be ignored. The layer is capped by a discontinuous jump in potential temperature $\Delta\theta$ which appears in (1) through the reduced gravity, $g' = \dfrac{\Delta\theta}{\theta_0} g$. Above this inversion, the flow is again neutrally stable. Clearly, there may be significant differences between flow described by the shallow water equations and that described by the full equations. In particular, for realistic atmospheric flows, the air is continuously stratified both above and below the inversion, variations in the phase of the waves beneath the inversion may be significant, and the inversion has finite thickness. Nevertheless, we believe that the qualitative resemblence of the flow in Figs. 9 and 10 to hydraulic flow is sufficient to merit a more detailed comparison.

We solve eqs. (1) and (2) numerically, using second-order centered finite differences for spatial derivatives and lepfrog time differencing. We impose a radiation condition which eliminates artificial reflections at the lateral boundaries by advecting the outgoing gravity-wave

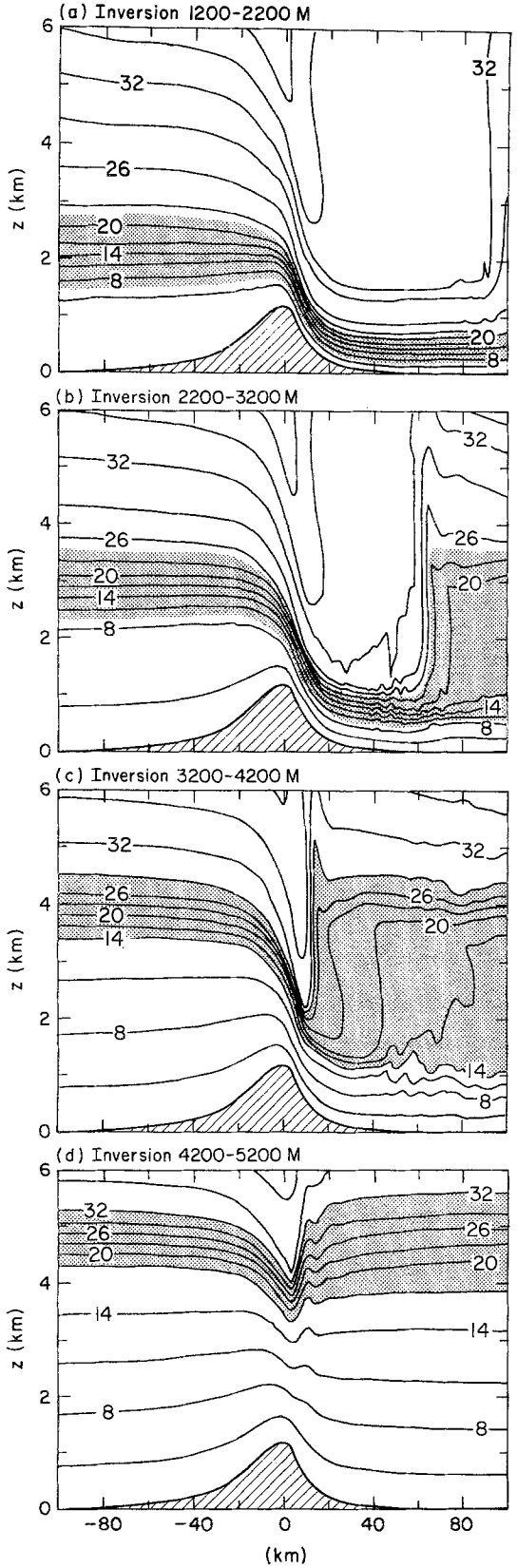

Fig. 9. Potential temperature contours (°C) at $t = 20000$ s for simulations with $H_m = 1200$ m, $U_1 = U_2 = U_3 = 20$ m s^{-1}, $N_1 = N_3 = .011$ s^{-1}, $N_2 = .0239$ s^{-1}, and the inversion layer located at (a) 1200–2200 m, (b) 2200–3200 m, (c) 3200–4200 m, and (d) 4200–5200 m. The shaded area highlights the location of the inversion layer

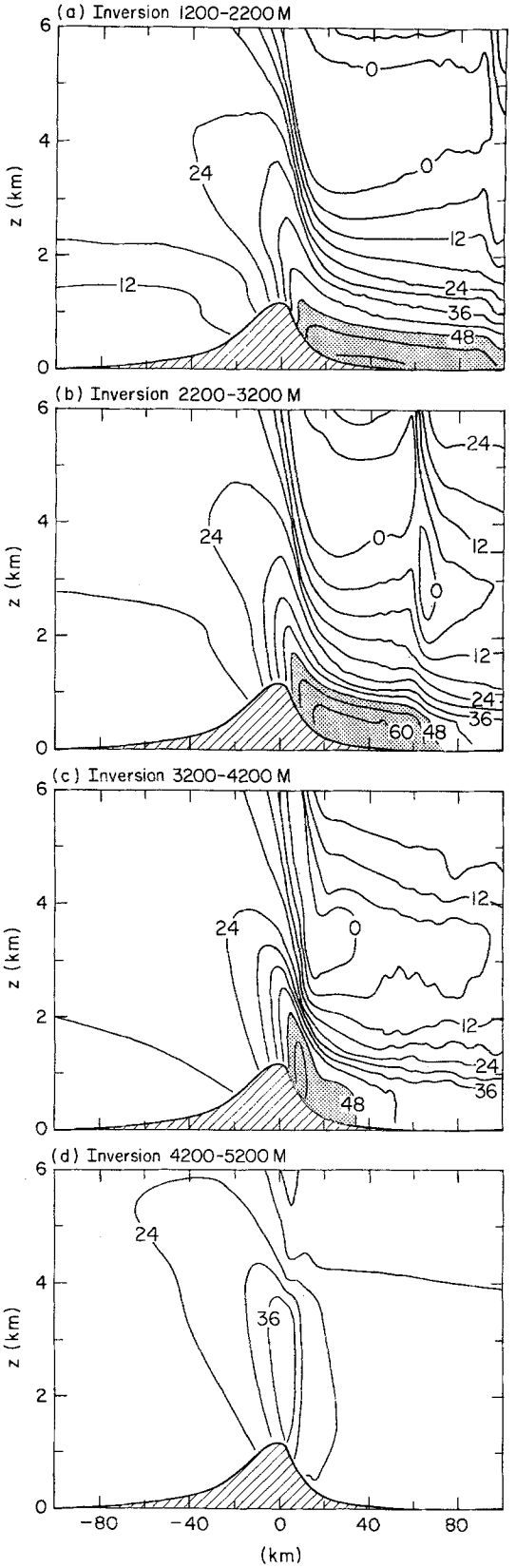

Fig. 10. As in Fig. 9, except for horizontal velocity field (in m s^{-1}). The shaded area denotes the region in which the winds exceed 48 m s^{-1}

mode through the boundary with its correct phase speed. Thus, at the lateral boundaries, we replace the momentum equation (1) with

$$\frac{\partial \phi}{\partial t} + (u \pm \sqrt{g'h}) \frac{\partial \phi}{\partial x} = 0 , \qquad (3)$$

where the ± sign is used at the downstream or upstream boundary, respectively. The numerical solution of (1) and (2) conserves both mass and momentum across any hydraulic jumps that occur within the domain. We include a small damping term on the right hand side of eq. (1) to permit energy dissipation within the jumps, this has little effect on the simulation elsewhere. We have verified the accuracy of this model through comparisons with analytical solutions for steady (or steadily propagating) hydraulic jumps produced by a mountain barrier (cf. Houghton and Kasahara 1969).

In order to apply this hydraulic model to the continuously stratified flows shown in Fig. 9, we specify an initial wind $U = 20$ m s^{-1} and an inversion height H, equal to the height of the top of the undisturbed inversion layer. Based on the 15 °C potential temperature change across the continuously stratified inversion, we set $g' = .5$. We then integrate the hydraulic model for the same time ($t = 20\,000$ s) as in the continuously stratified model. The results for each of the 4 inversion heights are displayed in Fig. 11a.

In the shallow water layer simulation with the lowest inversion layer ($H_i = 2200$ m), the flow becomes supercritical ($F = u/\sqrt{g'h} > 1$) as it passes over the mountain crest, shoots down the lee slope, and then recovers through a hydraulic jump which propagates downstream continuously (Fig. 11a). For $H_i = 3200$ m, the jump propagates rapidly to a location near the base of the lee slope, and then becomes quasi-stationary. For $H_i = 4200$ m, the jump remains stationary over the central portion of the lee slope. When we increase the initial height of the inversion to $H_i = 5200$ m, the flow remains subcritical and the inversion layer dips only slightly as it traverses the mountain.

The formation and propagation of hydraulic jumps are governed by two dimensionless parameters, the upstream Froude number $F_0 = U/\sqrt{g'H_i}$ and the ratio of the maximum mountain height to the inversion depth $M_c = H_m/H_i$. For steady-state flows (or flows with steadily propagating jumps), stationary and propagating hydraulic jumps occur over the parameter ranges of F_0 and M_c shown in Fig. 12, which is taken from Houghton and Kasahara (1969). We have also plotted, in Fig. 12, the 4 points (F_0, M_c) which correspond to the 4 simulations shown in Fig. 11a. As the height of the inversion layer H_i increases, the point characterizing the flow shifts toward the origin in Fig. 12. Thus, the hydraulic solution shifts from a propagating jump (point A in Fig. 12), to a jump which is just stationary at the base of the lee slope

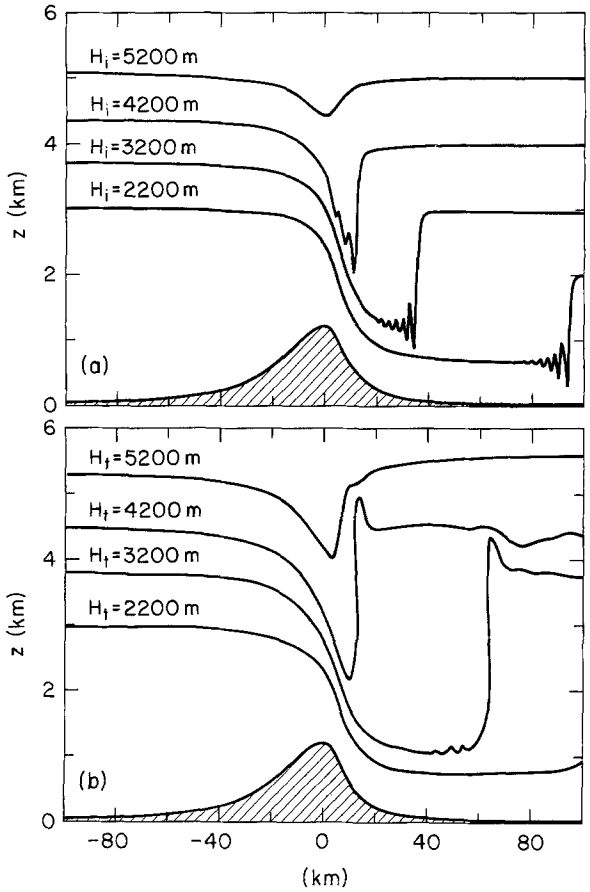

Fig. 11. (a) Heights of the inversion layer obtained from solutions to the shallow water equations at $t = 20\,000$ s for initial inversion heights $H_i = 2200$, 3200, 4200, and 5200 m. (b) Potential temperature contour located at the top of the inversion layer from each of the four cases presented in Fig. 9. The initial heights of the contours are $H_t = 2200, 3200, 4200$, and 5200 m

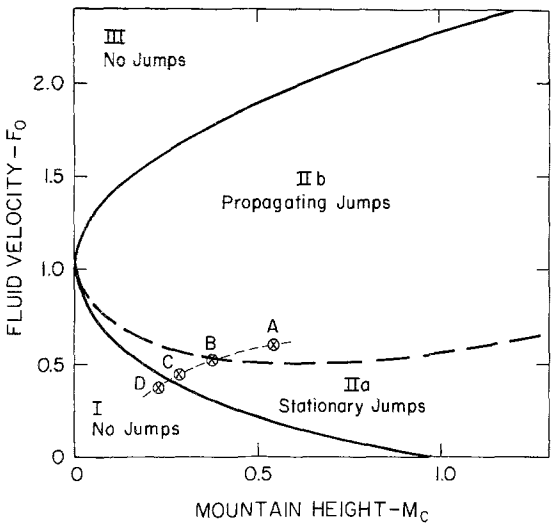

Fig. 12. Classification of flow conditions for asymptotic solutions to the shallow water equations as a function of the initial Froude number F_0 and dimensionless mountain height M_c. The crossed circles labeled A, B, C, and D correspond to cases simulated in Fig. 11a for H_i = 2200, 3200, 4200, and 5200 m, respectively (after Houghton and Kasahara 1969)

(point B), to a jump which remains just to the lee of the mountain crest (point C), and finally to no jump (point D) as the inversion height increases.

The potential temperature contours which define the top of the inversion layer in the continuously stratified simulations are plotted in Fig. 11b. They exhibit remarkable similarities to the hydraulic flow structures in Fig. 11a. The jump-like feature in the inversion layer propagates downstream in simulations with the lower inversion heights (H_t = 2200 and 3200 m), remains stationary over the lee slope when the inversion top is raised to 4200 m, and then disappears altogether in the simulation with H_t = 5200 m.

6. Summary and Conclusions

We have presented numerical simulations of the 15 April 1982 Bora, and shown that they are in good agreement with aircraft data gathered during that event. Our simulations suggest that, in this case, the factor which contributed most directly to the development of strong lee slope winds was the wave overturning region which formed beneath the inversion layer. When overturning occurs beneath the inversion, the low-level response is decoupled from the inversion, and it is the internal stratification, not the rapid change in density across the inversion, which is primarily responsible for the generation of the high surface wind speeds. Overturning is likely to dominate the dynamics whenever the cross-mountain flow is weak. In these situations, $N_1 H_m / U_1$ will be large (indicating that the wave amplitude will be sufficient to produce breaking), and the vertical wavelength $2\pi U_1 / N_1$ will be small (increasing the chance that the height at which the wave will break will lie below the inversion). This may be a common situation in the case of the Bora since the initial cross-mountain flow, which appears to be generated primarily as an ageostrophic response to pressure gradients associated with the advance of a cold air mass into the region northeast of the Dinaric Alps, is often rather weak.

The simulations described in section 5 suggest that when overturning does not occur beneath a strong inversion layer, the wave structure may be governed by hydraulic flow dynamics. This situation arises when the parameter $N_1 H_m / U_1$ is less than the value required to produce overturning or when the inversion layer is below the level at which overturning would occur.

The strong lee-slope shooting flow produced by wave overturning (see Figs. 4 and 6) appears to be qualitatively similar to the lee-slope response produced in the hydraulic-like flow driven by a strong inversion layer (see Figs. 9 and 11). Durran (1986) has investigated the strong downslope windstorms produced in numerical simulations of nonlinear mountain waves in atmospheres both with and without inversion layers. He demonstrated that the presence of either an inversion layer or wave overturning can produce a shooting flow over the lee slope which is dynamically analogous to hydraulic flow. Smith (1985) has presented an analytic model linking downslope windstorms to breaking waves in a continuously stratified atmosphere by solving Long's equation

subject to the assumption that the overturning region is well mixed so that the density in that region is constant. He found special solutions that exhibit a transition to shooting flow over the mountain crest which appear to be analogous to the transition to super-critical flow in hydraulic theory.

These studies all suggest that the shooting flows produced by hydraulic theory and those produced by wave breaking, may be fundamentally similar. However, it is important to distinguish between these two mechanisms when attempting to derive criteria for forecasting the Bora, or when describing the detailed dynamics of the flow.

In contrast to the Bora, downslope windstorms (chinooks) occur along the eastern slope of the Rocky Mountains when there is a strong cross-mountain flow throughout the troposphere. Because of this, as well as the fact that the Bora brings a sharp drop in temperature while the chinooks usually produce a pronounced warming, there has been a tendency to assume that these two wind situations are driven by different dynamical processes. However, observations (Lilly 1978) and numerical simulations (Peltier and Clark 1979; Durran and Klemp 1983) of the windstorm in Boulder, Colorado on 11 January 1972 suggest that the wave structure exhibited overturning and a strong lee-slope shooting flow similar to that shown in Figs. 4 and 6. Recent numerical simulations (Durran 1986) have also demonstrated that inversions in the flow upstream of the Colorado Rockies can generate hydraulic-like shooting flows without wave overturning, in a manner similar to that shown in Figs. 9 and 11. Thus, there is mounting evidence that the chinooks are produced by a transition to shooting flow which is similar to that which occurs in the Bora.

Acknowledgements

The authors wish to express their gratitude to Bruce Scharf, who assisted in conducting the numerical simulations for this research. Dale Durran's research was conducted in support of NSF Grant ATM-8320695 and as a summer visitor to the Mesoscale Research Section at the National Center for Atmospheric Research. NCAR is sponsored by the National Science Foundation.

References

Arakawa S (1969) Climatological and dynamical studies on the local strong winds, mainly in Hokkaido, Japan. Geoph Mag 34:359–425

Ball FK (1956) The theory of strong katabatic winds. Austrail J Phys 9: 373–386

Brinkmann WAR (1973) A climatological study of strong downslope winds in the Boulder area. NCAR Cooperative Thesis No 27, University of Colorado, p 229

Durran DR (1986) Another look at downslope windstorms. J Atm Sci, in review

Durran DR, Klemp JB (1982) The effects of moisture on trapped mountain lee waves. J Atm Sci 39: 2490–2506

Durran DR, Klemp JB (1983) A compressible model for the simulation of moist mountain waves. J Atm Sci 111: 2341–2361

Houghton DD, Kasahara A (1968) Nonlinear shallow fluid flow over an isolated ridge. Commun Pure Appl Math 21: 1–23

Kennedy PJ (ed) (1982) An ALPEX aircraft atlas. National Center for Atmospheric Research, Boulder, Colorado, July 1982, p 226

Klemp JB, Durran DR (1983) An upper boundary condition permitting internal gravity wave radiation in numerical mesoscale models. Mon Wea Rev 111: 430–444

Kuettner J (1959) The rotor flow in the lee of mountains. GRD Research Notes No 6, Geophysical Research Directorate, Air Force Cambridge Research Center, Bedford, Mass.

Lilly DK (1978) A severe downslope windstorm and aircraft turbulence event induced by a mountain wave. J Atm Sci 35: 59–77

Lilly DK, Klemp JB (1979) The effects of terrain shape on nonlinear hydrostatic mountain waves. J Fluid Mech 95: 241–262

Long RR (1953) A laboratory model resembling the "Bishop-wave" phenomenon. Bull Am Met Soc 5: 205–211

Peltier WR, Clark TL (1979) The evolution and stability of finite-amplitude mountain waves. Part II: Surface wave drag and severe downslope windstorms. J Atm Sci 36: 1498–1529

Schweitzer H (1953) Versuch einer Erklärung des Föhns

als Luftströmung mit überkritischer Geschwindigkeit. Arch Met Geoph Biokl A5: 350–371

Smith RB (1982) Aerial observations of the Yugoslavian Bora: Preliminary results. ALPEX Preliminary Scientific Results, GARP-ALPEX No 7, World Meteorological Organization, Geneva, Switzerland, December, 1982, pp 187–201

Smith RB (1985) On severe downslope winds. J Atm Sci 42: 2597–2603

Yoshino MM (1976) Local wind Bora. University of Tokyo Press, p 189

Authors' addresses: Dr. Joseph B. Klemp, NCAR, P.O. Box 3000, Boulder, CO 80307-3000, U.S.A.; Dr. Dale R. Durran, Department of Meteorology, University of Utah, 819 Wm. C. Browning Building, Salt Lake City, UT 84112, U.S.A.